Computers & Geosciences 93 (2016) 1–11

Contents lists available at ScienceDirect

Computers & Geosciences

journal homepage: www.elsevier.com/locate/cageo

Case study

Volcanic edifice alignment detection software in MATLAB: Test data and preliminary results for shield fields on Venus

Bradley J. Thomson [a,*], Nicholas P. Lang [b]

[a] Center for Remote Sensing, Boston University, 725 Commonwealth Ave., Boston, MA 02215, USA
[b] Department of Geology, Mercyhurst University, 501 E. 38th St., Erie, PA 16546, USA

ARTICLE INFO

Article history:
Received 14 October 2015
Received in revised form
20 April 2016
Accepted 22 April 2016
Available online 25 April 2016

Keywords:
Spatial distribution
Software
Anisotropy
Shield fields
Volcanology
Magellan

ABSTRACT

The scarcity of impact craters on Venus make it difficult to infer the relative ages of geologic units. Stratigraphic methods can be used to help infer the relative ordering of surface features, but the relatively coarse resolution of available radar data means ambiguity about the timing of certain features is common. Here we develop a set of statistical tools in MATLAB to help infer the relative timing between clusters of small shield volcanoes and sets of fractures in the surrounding terrain. Specifically, we employed two variants of the two-point azimuth method to detect anisotropy in the distribution of point-like features. The results of these methods are shown to successfully identify anisotropy at two spatial scales: at the whole-field level and at scales smaller than a set fraction of the mean value. Initial results on the test cases presented here are promising, at least for volcanic fields emplaced under uniform conditions. These methods could also be used for detecting anisotropy in other point-like geologic features, such as hydrothermal vents, springs, and earthquake epicenters.

1. Introduction

Absent returned samples, the two methods of remotely inferring the ages of planetary surfaces are to measure the spatial density of impact craters and to examine stratigraphic cross-cutting relationships. Venus possess a dearth of the former and an abundance of the latter, meaning that relative age assessments are possible but it is difficult to correlate surface ages between distant geologic units that do not share a common set of cross-cutting structures.

Impact craters do provide some general insight about the geologic history of Venus; the small number of impact structures evident planet-wide necessitate one or more episodes of massive resurfacing (e.g., Phillips et al., 1992; Schaber et al., 1992; Strom et al., 1994). Obtaining absolute ages on Venus using craters, however, is akin to dating Earth's oceanic crust using only impact craters. While the paucity of craters are indicative of the ocean basins' youthfulness, outside of a few rare recognized impact structures (e.g., Chicxulub, Mjolnir, Chesapeake Bay), the density of craters is insufficient to provide age controls on sub-divisions of units.

Here, we seek to provide insight into an aspect of the stratigraphy of Venus by using a set of statistical tools to infer the relative timing between clusters of shield volcanoes and sets of fractures in the surrounding terrain. In particular, we employ the two-point azimuth method (Lutz, 1986) to look for anisotropy in the distribution of shields, and then determine if the inferred directionality (if present) corresponds to particular set(s) of structures, thus implying relative timing between the two. This contribution presents a software package to accomplish this task and provides some proof-of-concept examples; further results are expanded upon in a companion paper (Lang and Thomson, 2016 in prep.).

2. Background

2.1. Potential tectonic influence on the localization of volcanism

Many workers have noted the potential of tectonic factors to influence the style and development of volcanic vents and dikes. For example, the geometry of far-field portions of radiating dike swarms appear to be controlled primarily by the orientation of the regional maximum horizontal compressive stress (e.g., Anderson, 1951; Odé, 1957; Ernst et al., 1995). This notion is based upon the observation that failure in extension occurs in planes that are normal to the least principal stress, forming mode I fractures. In a similar vein, alignments of volcanic vents have been suggested to be indicative of structural control, with their distribution possibly reflecting the stress regime of the upper crust (e.g., Kear, 1964;

* Corresponding author.
E-mail address: bjt@bu.edu (B.J. Thomson).

http://dx.doi.org/10.1016/j.cageo.2016.04.012
0098-3004/

Nakamura, 1977; Connor, 1990; Cebriá et al., 2011). As with dikes, emplaced features tend to be arrayed in lines that are normal to the inferred minimum horizontal compressive stress. A complicating factor with point-like vents is that, unlike a dike, they may be emplaced over a longer period of time, and thus may be reflective of potentially evolving regional stress. As discussed below in Section 5.1, a disagreement between the two methods used in this work may be indicative of changing tectonic and stress conditions.

2.2. Shield field characteristics and importance

Small shield volcanoes represent perhaps the most dominant manifestation of volcanism on Venus. Shields are extrusive volcanic constructs <20 km in diameter (average of ~1–2 km in diameter) that are cone, flat topped, dome, or shield shaped, and «1 km in height (Aubele and Sliuta, 1990; Guest et al., 1992; Crumpler et al., 1997). Shield fields are enhanced concentrations of shields, typically tens to hundreds of edifices, that range in density from 4 to 10 edifices per 10^3 km^2 within an area of $\sim 10^4$ km^2 (Crumpler et al., 1997). Clusters of small volcanoes are present also on the Earth (e.g., Connor and Conway, 2000), Mars (e.g., Hodges and Moore, 1994; Bleacher et al., 2009; Richardson et al., 2013), and the Moon (e.g., Basaltic Volcanism Study Project, 1981) and, in each case, likely reflect small batches of magma tapped at low rates from their presumably mantle source region (e.g., Crumpler et al., 1997). This is likely the case for venusian shield fields as well, which tend to be roughly equant in outline with diameters ranging from 50 to ~1000 km.

Because of their widespread occurrence across the surface, understanding the timing of venusian shield emplacement is critical for unraveling Venus' volcanic history. Yet there remains disagreement about the relative age assignments given to many shield fields. At least two major investigations into the stratigraphic relationships between shield fields and their local surroundings have reached diametrically opposed conclusions (Addington, 2001; Ivanov and Head, 2004). Addington (2001) examined 179 shield field clusters and found that 42% appear to be younger than or postdate the regional plains, 10% contain some indications that they are older, and 47% are ambiguous (i.e., no clear stratigraphic relationships could be inferred). In contrast, Ivanov and Head (2004) examined 141 shield fields and found that 69% of shield fields appeared to be older than or predate regional plains, 8% postdate, and 25% are either ambiguous or synchronous.

Part of this discrepancy may be due to the difficulty in trying to discern small-scale geologic contact relationships at or below the limits of resolution, which is 75 m for Magellan full-resolution SAR (synthetic aperture radar) data. To help address this concern, we have undertaken an independent examination of the spatial distribution of individual edifies in shield fields to determine if there are preferred alignments, and, if so, determine the relationship between these alignments and local stress conditions as determined from fractures, wrinkle ridges, and other stress-strain markers.

3. Method

3.1. Two-point azimuth method (lutz)

In this work, we focus on azimuth methods that were initially developed by Lutz (1986) to quantify preferred orientations in clusters of terrestrial point-like features. In this method, the azimuth or orientation between each feature and all of the other points in a population are determined. For N points, there are $N(N-1)/2$ such orientations. The results are binned into a histogram

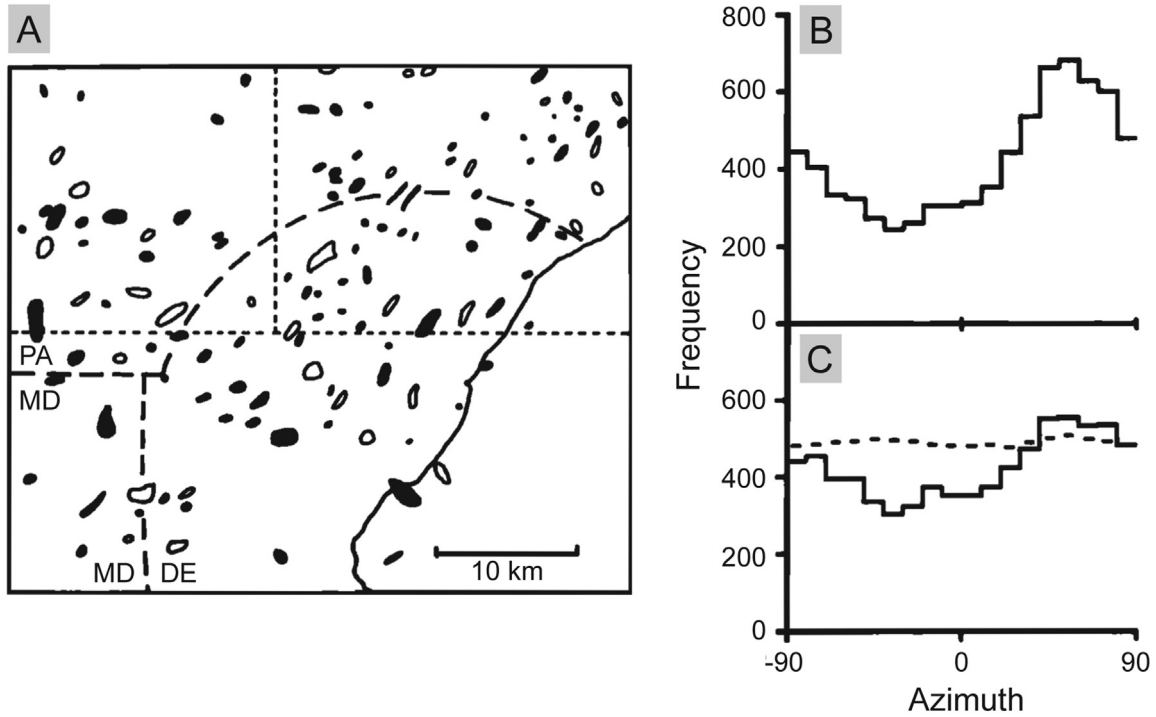

Fig. 1. (a) Map of magnetic anomalies in the Pennsylvania, Maryland, and Delaware region (from Lutz (1986), their Fig. 13 after Thompson and Hager (1977) their Fig. 9). The centroids of the 125 features were used in Fig. 1b–c. (b) Raw distribution of azimuth values binned into 10° intervals (from Lutz (1986), Fig. 14(a). (c) Corrected azimuth distribution; dashed line indicates 95% threshold value (mean+2σ) (from Lutz (1986), Fig. 14b).

or rose diagram, and peaks in the histogram indicate preferred alignments of features (Fig. 1). In order to control for field shape, i.e., the distribution of points as defined by the closed polygon containing them, the observed distribution is compared to a Monte Carlo model. Specifically, the raw histogram is normalized by the mean result of a family of models generated using Monte Carlo techniques, each of which has a random distribution of the same number of points in a model space of similar spatial extent (Lutz, 1986).

3.2. Modified two-point azimuth method (Cebriá)

Several refinements to this method have been proposed. For example, since the method assumes that the alignment of features is spatially homogeneous (i.e., it does not vary across the field), alignments between subregions or subpopulations with different characteristics are neglected or not captured. Similarly, alignments at different spatial scales are also not resolved. To address these concerns, Lutz and Gutmann (1995) modified the azimuth method to examine alignments as a function of scale, and Hammer (2000) calculated azimuths between nearest-neighbors to assess preferred alignments on the most local scale.

A recent modification to the azimuth model was implemented by Cebriá et al. (2011) on edifice orientations in the Michoacán-Guanajuato Volcanic Field in Mexico and Calatrava region in Spain. In this model, the azimuth calculations were constrained to lines that connect vents that lie relatively close together (Fig. 2). Here, the term "relatively close together" refers to an empirically-determined value considered to be the minimum significant distance, d_{ms}, which assumed to be less than one-third of the standard deviation (σ) from the mean separation distance ($\bar{x}$), i.e., $d_{ms} \leq |\bar{x} - 1\sigma|/3$.

These modified two-point azimuth method results given in Fig. 2c support a dominance of NE-directed lineaments for the region, with a prevalent orientation at ~N30°E. If the relatively low frequencies shown by the NW-directed azimuths are considered, other secondary lineaments can be interpreted at ~280° and ~305°. These results are significant because the more prominent volcanic edifice alignment seems to be related to older fracture zones that show evidence of present reactivation. Since the NE-oriented fracture zones display a dip-slip component, they may be more favorable at producing space accommodation for magma ascent (Cebriá et al., 2011).

3.3. Implementation in MATLAB

We have implemented the original two-point azimuth method (Lutz, 1986) and a second modified two-point azimuth algorithm to focus on smaller spatial scales (Cebriá et al., 2011) in a single graphical user interface (GUI) built using MATLAB (MATrix LABoratory) software. In the GUI, the user ingests a pre-prepared text file that is a 2-column listing of the center latitude and longitude of each volcanic construct. Inputting the point data as decimal degrees rather than Cartesian *x, y* distances implicitly avoids introducing distortion due to planetary curvature. The software has been configured so that the user can designate the planetary body of interest (Earth, Venus, Mars, or a unit sphere). The main body of the GUI consists of three panels (Fig. 3), and the sequence of processing steps in given in the flowchart in Fig. 4 and listed in Table 1. In the left-most panel in Fig. 3, the distribution of point features (e.g., shields) can be visually confirmed in a lat-lon scatter plot. The middle panel displays a raw, uncorrected histogram of orientation measurements. These measurements utilize the MATLAB function "azimuth," part of the Mapping Toolbox, which determines the azimuth between two points on a given ellipsoid. In the right-most panel, the user specifies the number of Monte Carlo

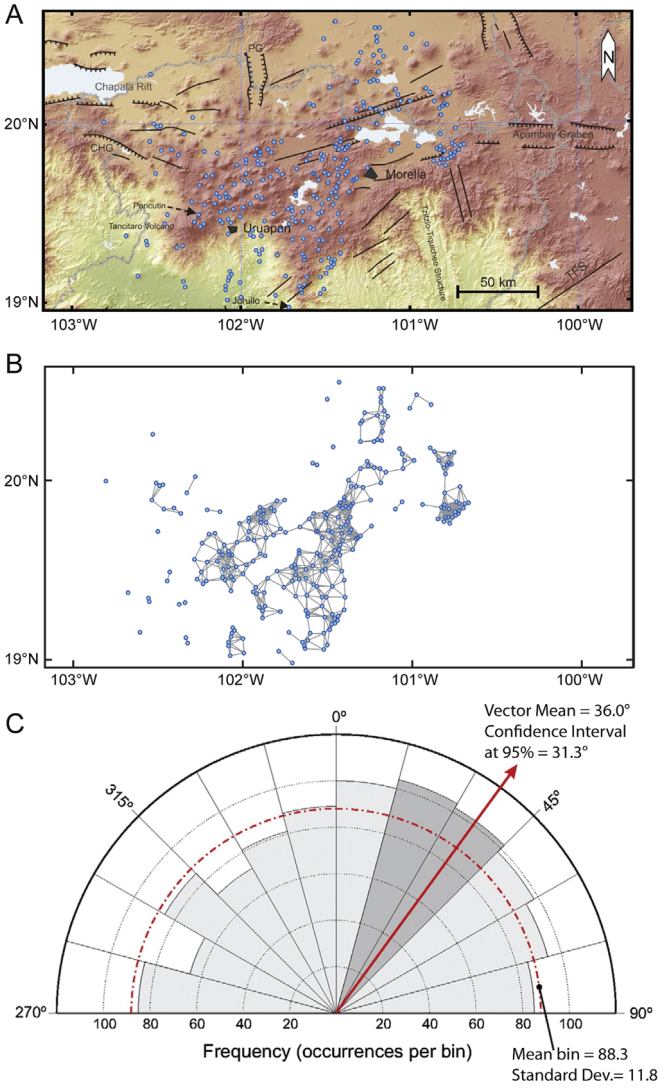

Fig. 2. (a) Shaded relief map of the Michoacán-Guanajuato Volcanic Field with the main Cenozoic tectonic features and the distribution of Pliocene to present day monogenetic vents in the volcanic field (modified from Cebriá et al. (2011)). CHG = Cotija half-graben, PG = Penjamillo graben. (b) Distribution of modified two-point azimuth model with line segments ≤ 12 km (i.e., $\leq |x - 1\sigma|/3$) where a general tendency towards NE-directed lineaments can be observed (after Cebriá et al. (2011)). (c) Corresponding rose diagram at 15° bin intervals (frequency as number of occurrences per bin) for azimuths mapped in Fig. 3b. Dark gray bins are those with frequencies higher than one standard deviation above the mean (from Cebriá et al. (2011)).

models to run. Each model randomly places an equivalent number of shields within a region identical in shape to the original, and the results from these empirical distributions are used to correct for the effect of field shape and also determine if the observed distribution is consistent with a random distribution. There are five basic steps in the Monte Carlo model. First, the bounding region is defined by the edge edifices, which delineate the convex hull or convex envelope. Second, this convex hull is divided into a set of constituent triangles using a Delaunay triangulation (e.g., Lee and Schachter, 1980). Next, we compute the area of each triangle, and assign it a weighting factor that is proportional to its area. Finally, the position of each random point x in a given triangle is determined by generating two random numbers a_1 and a_2 to calculate $x = a_1(v_1 - v_0) + a_2(v_2 - v_0)$, where v_0, v_1, and v_2 are vertices of the triangle (Weisstein, 2016).

Upon execution, a "normalized" histogram is produced from the Monte Carlo results whereby each histogram cell is set equal to the expected value times the observed value divided by the mean value in the Monte Carlo runs (Eq. (1), after Lutz (1986)).

$$\hat{z}_i = \left[\frac{\frac{N(N-1)}{2k}}{z_{MC-mean,\,i}} \right] z_{obs,\,i} \text{ for } i = 1 \text{ to } k \tag{1}$$

Here, $\hat{z}_i$ is the normalized value of the ith bin; N is the number

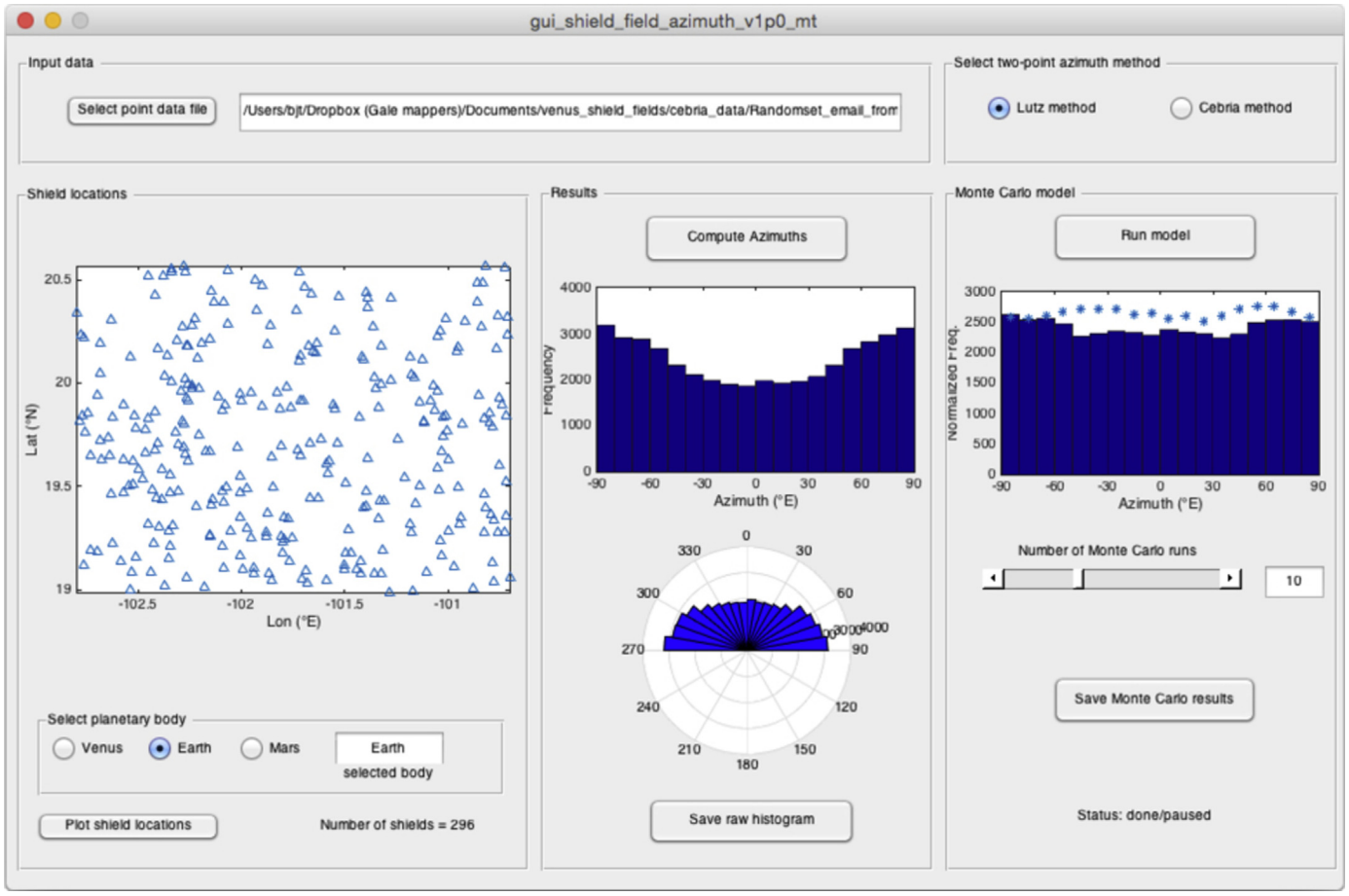

Fig. 3. Snapshot of MATLAB GUI implementing two-point azimuth model. Left panel gives scatterplot of random point data from Cebriá et al. (2011). In the middle panel, a raw histogram and corresponding rose plot are given. A "normalized" histogram via Monte Carlo model is given in the right panel. Note that as expected for a random distribution of points, none of the histogram bins exceed the critical threshold value (indicated by * symbols).

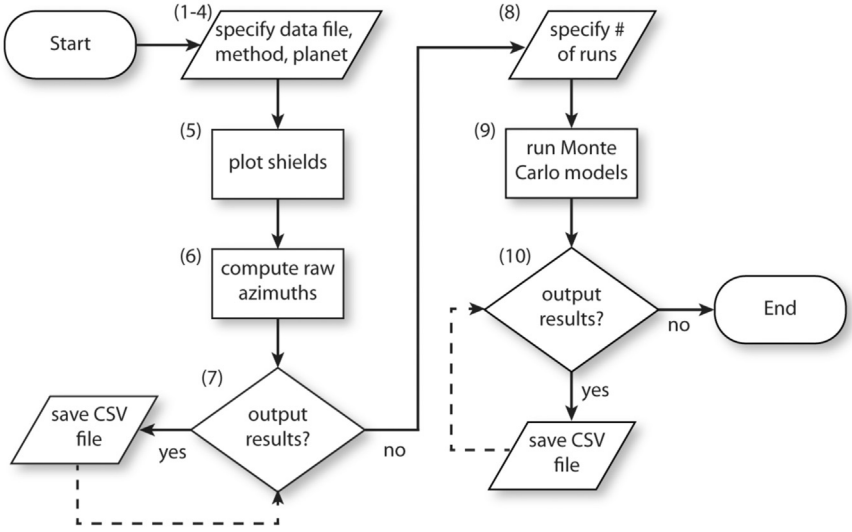

Fig. 4. This flowchart details the sequence of processing steps in the GUI to run the Lutz (1986) or Cebriá et al. (2011) two-point azimuth methods. Rounded squares give the starting and end points of the sequence. A parallelogram indicates an input or output operation, a rectangle indicates a data manipulation step, and a rhombus indicates a decision point. Numbers enclosed in parentheses correspond to the processing steps given in Table 1.

of points, the quantity $N(N-1)/2k$ is the expected value per bin; k is the number of bins (18 in this instance); $z_{MC-mean,i}$ is the mean value of the ith bin averaged from all of the Monte Carlo runs, and $z_{obs,i}$ is the observed histogram value of the ith bin. Note that to implement the Monte Carlo models for the Cebriá et al. (2011) method, the number of azimuths in each empirical distribution had to be fixed at the same number in the observed distribution.

To determine if a given normalized histogram value is statistically significant to the 95% significance level, the Student's t distribution is used to determine the 95th percentile critical threshold value, $\hat{L}_i$.

$$\hat{L}_i(\alpha) = \left[\frac{\frac{N(N-1)}{2k}}{z_{MC-mean,\,i}}\right]\left(z_{MC-mean,\,i} + \sigma_i\, tinv(\alpha, \nu)\right) \quad (2)$$

In Eq. (2), σ_i is the standard deviation of the mean value of the ith bin, α is the desired significance level, υ is one less than the number of Monte Carlo runs, and *tinv* is the Student's t inverse cumulative distribution function (an existing MATLAB function). Histogram values that exceed the critical threshold value ($\hat{L}_i$) are deemed statistically significant.

4. Results

4.1. Overview of results

In order to test the validity of these models, we have applied them to a terrestrial data set, a randomly generated point set, and two example from Venus. Results from each of these applications are given below.

4.2. Terrestrial example using data from Lutz (1986)

As a proof-of-concept, a data set from Lutz (1986) is reproduced in Fig. 5a–c. Data were processed in the GUI and exported to comma-separated value text files using the "Save raw histogram" and "Save Monte Carlo results" buttons in the middle and right-hand panels of the GUI, respectively (see button position in Fig. 3). Individual data points are given in Fig. 5a; raw histogram values

Table 1
Sequence of processing steps.

Step no.	Description
(1)	Click "select point data file" button to bring up file-selection dialog.
(2)	Navigate to chosen folder, select text file (*.txt) that is a two-column listing of center lat, lon points.
(3)	Select radio button indicating choice of two-point azimuth method: Lutz method (default) or Cebriá et al. method.
(4)	In left panel, select radio button for planetary body of interest (currently Venus, Earth, or Mars).
(5)	Click "Plot shield locations" button to create *x*–*y* plot of shield locations in left panel. Note this also served to verify that the point data file was ingested correctly.
(6)	In the middle panel under "Results," select the "Compute Azimuths" button. This computes a "raw" two-point azimuth method or Cebriá et al. method, and displays the results in a histogram and rose diagram.
(7)	[Optional] Data from the raw histogram can be saved in comma-separated value (csv) format by clicking on the "Save raw histogram" button at the bottom of the middle panel.
(8)	In the right-most panel within the "Monte Carlo model" button group, the user specifies the number of Monte Carlo runs desired using either the bar slider or by entering an integer value into the text field to the right of the slider. The default value is 10, although the recommended minimum number of runs is 100.
(9)	The user then clicks the "Run Model" button on the right panel to execute the specific number of Monte Carlo runs.
(10)	[Optional] Similar to step #7 data from the normalized histogram can be saved in csv format by clicking on the "Save Monte Carlo results" button at the bottom of the right panel.

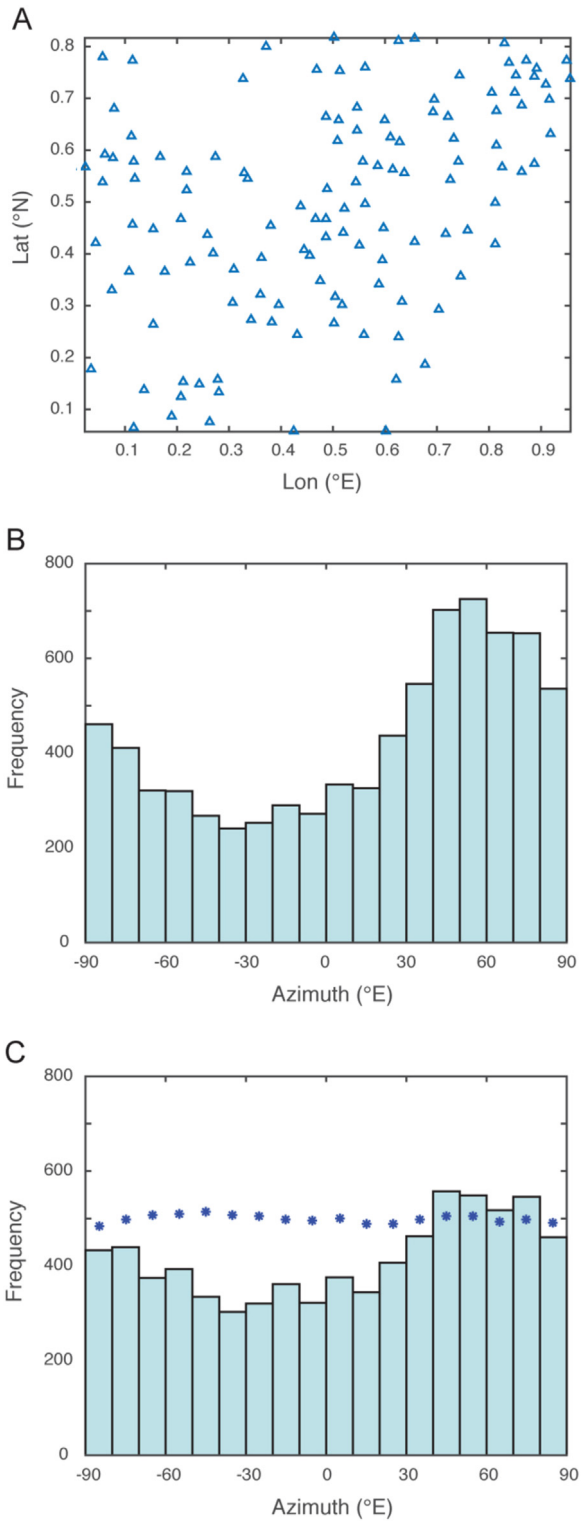

Fig. 5. (a) Centroids positions of magnetic anomaly contour closures in the Pennsylvania, Maryland, and Delaware region (after Lutz (1986)). (b) Raw distribution of azimuth values binned into 10° intervals (compare with Fig. 1b). (c) Corrected azimuth distribution; overlain star symbols in each bin indicate the 95% threshold value (compare with Fig. 1c).

are given in Fig. 5b, and normalized histogram values are given in Fig. 5c. In the normalized histogram, four adjacent 10° bins centered on N60°E exceed the expectations of a random pattern at the 0.05 significance level (as indicated by blue asterisks). These results faithfully reproduce the original data in Fig. 1b and c and lend confidence the algorithm is executing as designed. Note since the points in this example are the centroids of magnetic anomalies, no age inferences can be made.

A critical factor illustrated by this example is the importance of designating the appropriate coordinate system of the data. The

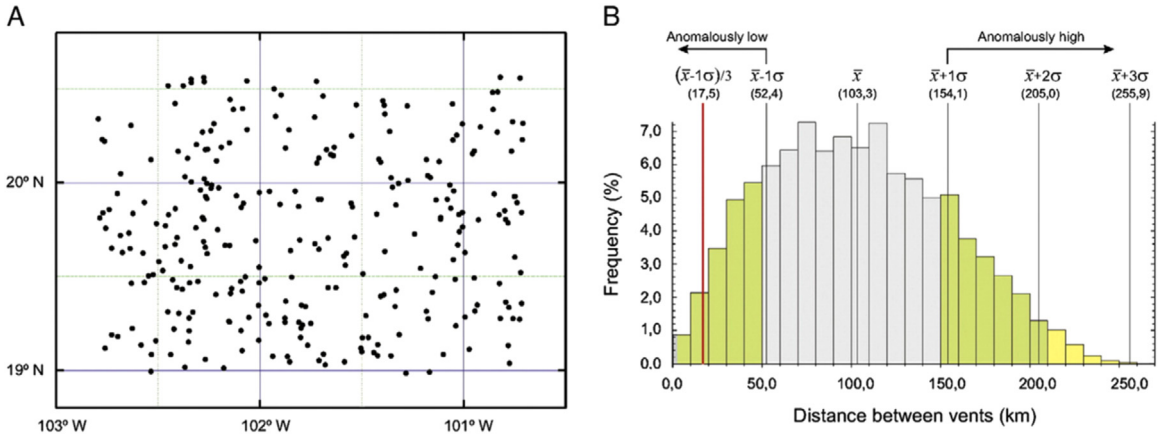

Fig. 6. (a) Randomized distribution of 296 points from Cebriá et al. (2011), their Fig. 1. (b) Frequency histogram (expressed as % of total population) of the lengths of all possible lines interconnected the points given in a.

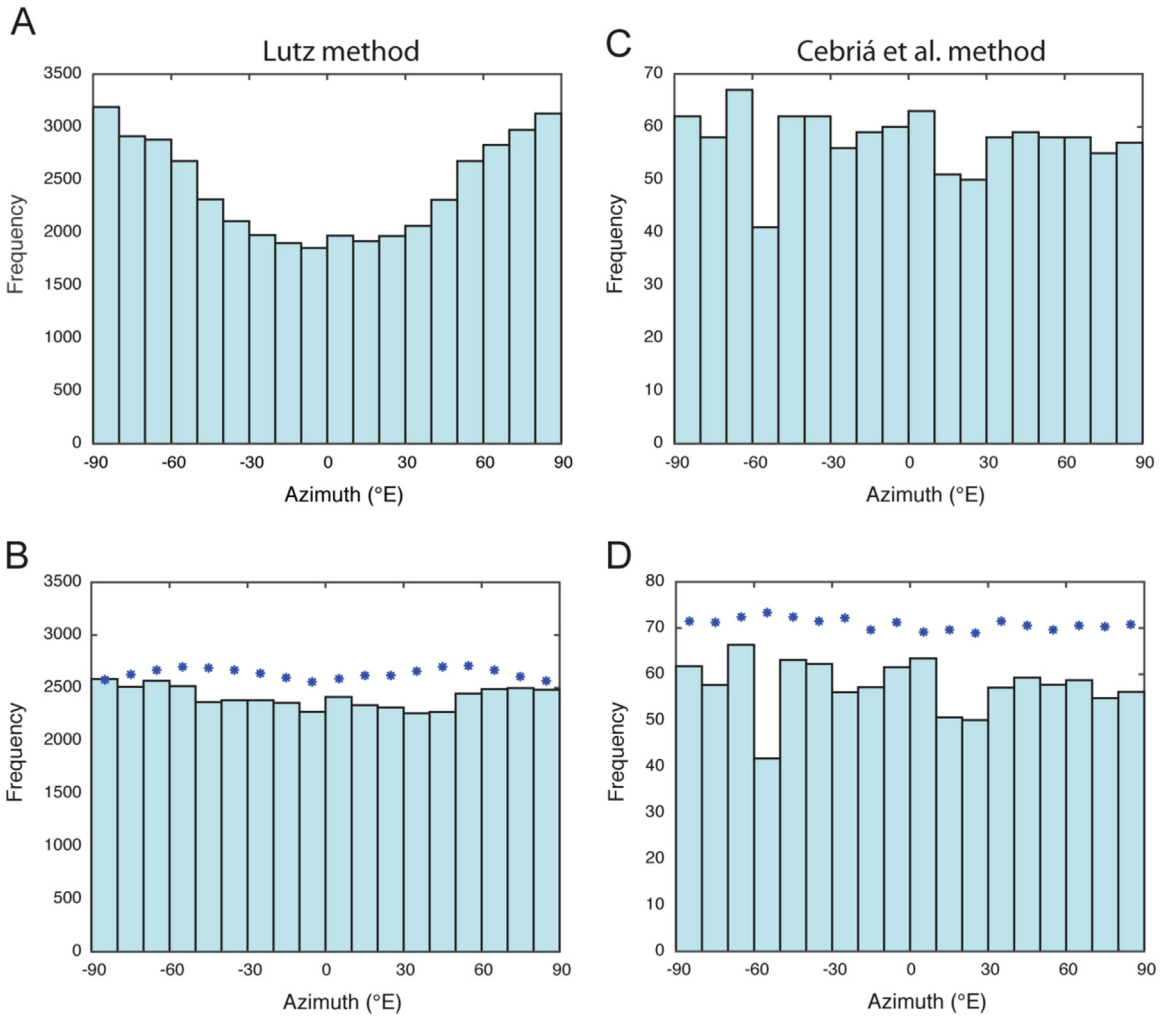

Fig. 7. Results from two-point azimuth methods for randomly placed point data in Fig. 6a. (a) Histogram of raw azimuth values using two-point azimuth method of Lutz (1986) with 10° bins. (b) Normalized two-point azimuth distribution from a; overlain star symbols in each bin indicate the 95% threshold value (mean+2σ). (c) Histogram of raw azimuth values using Cebriá et al. (2011) modified two-point azimuth method. (d) Normalized modified two-point azimuth distribution from c. Overlain star symbols in each bin indicate the 95% threshold value.

original figure from Lutz contained no boundary markings to indicate latitude or longitude. Coordinates could be inferred using the state boundary intersection points as known tie points, but when the feature centroids were extracted using these tie points and assuming Cartesian geometry, distortion due to the map projection (likely Mercator) is evident. For this example, points were arbitrarily assigned locations between 0–1°N lat, 0–1°E lon to preserve the original figure aspect ratio (width/height) of 1.18.

4.3. Null example using test data from Cebriá et al. (2011)

As a further test of the software functionality, we ran both components of MATLAB code using a randomly-generated set of point data from Cebriá et al. (2011). This test data set corresponds to a random distribution of 296 points in an area similar to the Michoacán-Guanajuato volcanic field in central Mexico. Fig. 6a gives an *x*–*y* scatterplot of these points; Fig. 6b gives a frequency histogram of distances between points (both figures are from Cebriá et al. (2011)). Fig. 3 is a screenshot of the MATLAB GUI using the Lutz (1986) method showing results for the same data given in Fig. 6a and b. Close-up views of the histogram panels are given in Fig. 7a–d. In the Lutz (1986) method, the raw histogram (Fig. 7a) reveals a broad mode centered at $\pm 90°$, an orientation consistent with the E–W elongation of the overall field shape. Normalizing the histogram with the results from the Monte Carlo model (Fig. 7b), however, indicates that this broad mode does not exceed the significance threshold (i.e., it is an artifact of the field shape). The raw histogram using the Cebriá et al. (2011) method is given in Fig. 7c, and the normalized histogram in given in Fig. 7d. As expected, no preferred orientations in the normalized histograms given in Fig. 7d exceed the critical threshold value, indicating there is no evidence for a strong preferred orientation as expected from a random distribution of points. As with the prior example, no age inferences are possible.

4.4. Venus example 1: Chernava Colles

Our first application of this model to Venus is at Chernava Colles, a 1000 km diameter shield field centered near 10.5°S, 335°E (Fig. 8) between Vasilisa Regio and Kanykey Planitia. It is located on northwest-trending fractures associated with Albasty Fossae and Gui Ye Chasma along which multiple coronae have formed and erupted numerous long lava flows. Bender et al. (2000) originally mapped Chernava Colles as part of an extensive regional plains unit that postdates much of the corona-related flow material in this area; the shield field was lumped with the regional plains unit and distinct shields and flow materials associated with the field were not distinguished. Shields within Chernava Colles are predominately cone-shaped and ~1–5 km in diameter, though several domical shields ≥ 5 km are also present. Cone-shaped shields typically lack noticeable summit pits and obvious associated flow materials, whereas the dome-shaped shields are more typically associated with summit pits and localized flow materials. Numerous shields within Chernava Colles occur directly on top of, and are mostly superposed on, the fractures. This suggests a genetic relation between the fractures and the shields where the fractures pre-date shield formation. Using a terrestrial analogy for the formation of cinder cones on Earth (e.g., Crumpler and Aubele, 2000), magma likely rose up preferentially along pre-existing fractures and erupted to create the individual shields. In this case, stratigraphic relationships between the shield field and surrounding materials are clearly defined and there is a well-preserved qualitative record of the broad-scale stress field orientation that likely existed when Chernava Colles was emplaced.

The results of running the statistical tool on Chernava Colles are given in Fig. 9. We mapped $N=604$ shields and ran 100 Monte

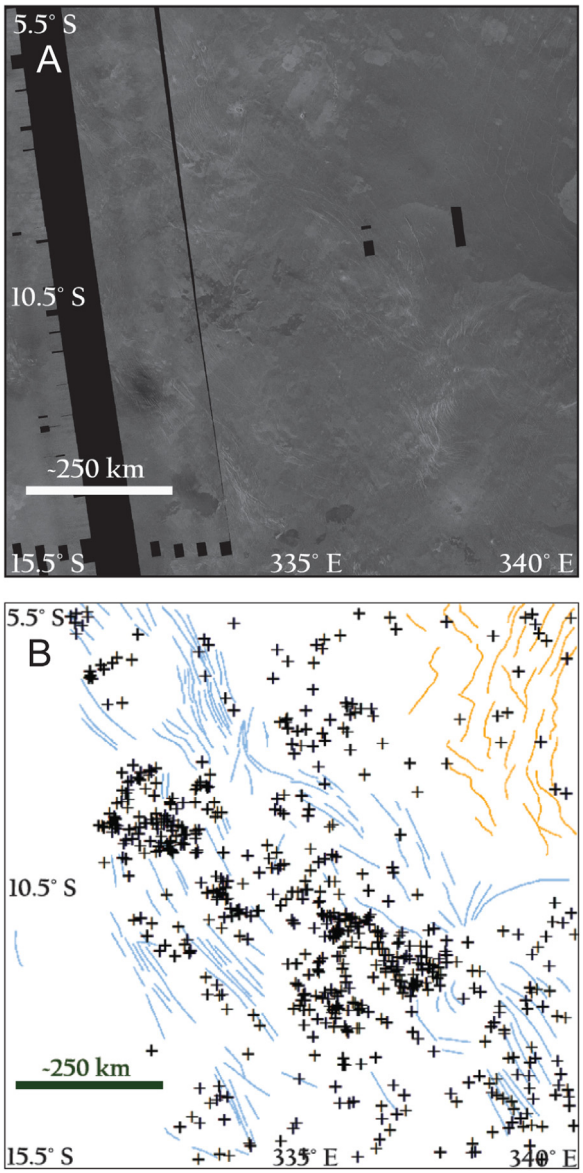

Fig. 8. (a) Magellan left-look SAR image of a portion of Chernava Colles centered at 10.5°S, 335°E. The top of the image is north. (b) Simplified geologic map of the same portion of Chernava Colles given above highlighting the distribution of small shields (black crosses). Blue lines represent fractures and orange lines represent contractional structures (wrinkle ridges). (For interpretation of the references to color in this figure legend, the reader is referred to the web version of this article.)

Carlo models. Results from the raw histogram using the Lutz method (Fig. 9a) indicate a strong overall NW to WNW trend for vent orientation at Chernava Colles. In the normalized histogram (Fig. 9b), a broad mode is present that extends from 40 to 70°W, all of which have values that exceed the 95th percentile critical threshold. This detected anisotropy is broadly consistent with the dominant fracture trend in Fig. 8b, where the majority of mapped fractures are oriented NW–SE. This would suggest that the shields are younger than the fractures, a relationship that is consistent with that inferred from geologic mapping alone. Results from the Cebriá et al. (2011) method are more difficult to interpret. The raw Cebria histogram in Fig. 9c is multi-modal; in the normalized histogram, three individual bins are at or slight above the 95th percentile critical threshold in Fig. 9d. Two of these (30–40 °W and 60–70°W) fall within the broad mode indicated in the Lutz

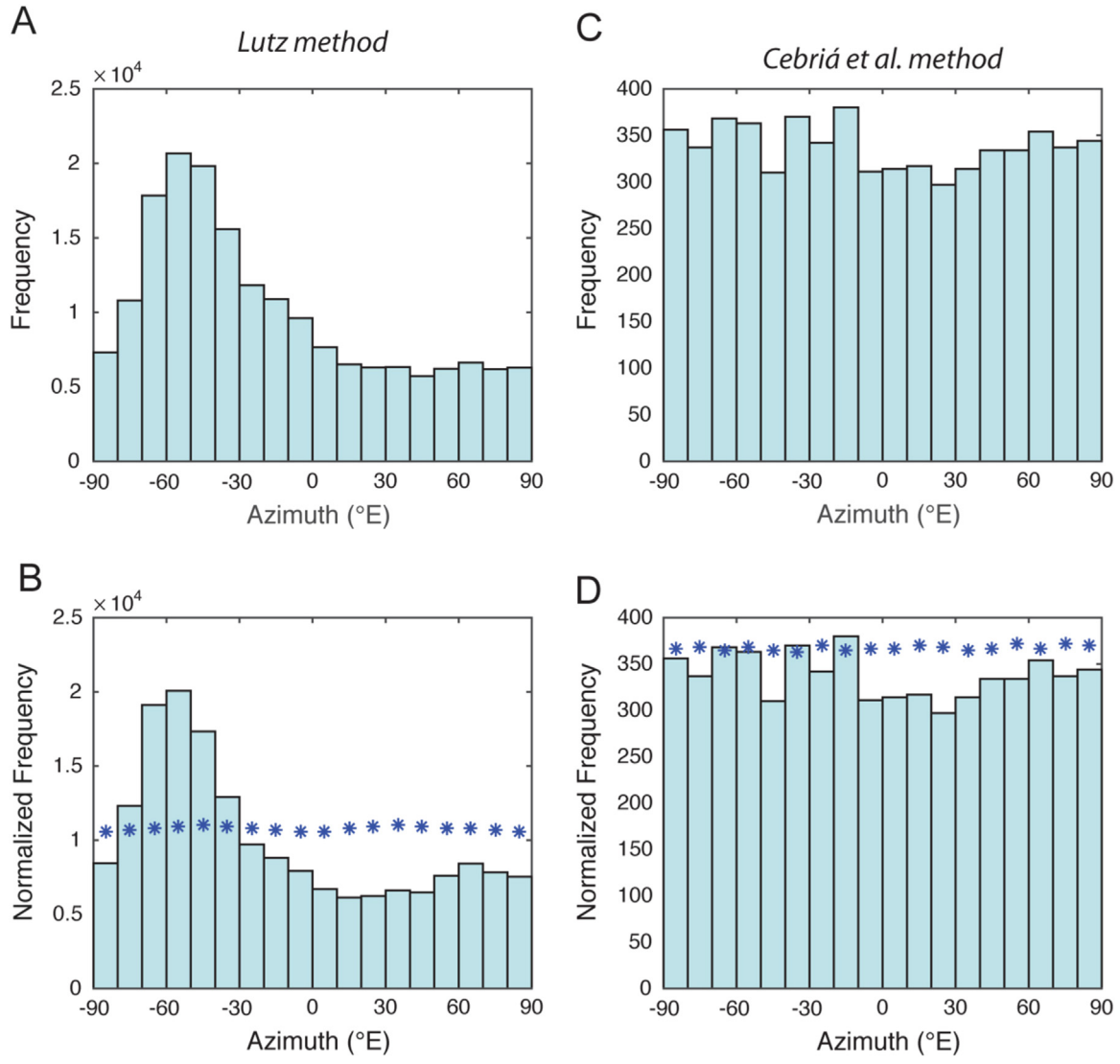

Fig. 9. Comparison of output of Lutz (1986) and Cebriá et al. (2011) models for Chernava Colles ($N=604$ shields). (a) Raw histogram in *Lutz* method. (b) Normalized histogram, *Lutz* method. Blue stars indicate 95% significance threshold. (c) Raw histogram of azimuths that fall within *Cebriá* et al. method cutoff. (d) Normalized histogram, *Cebriá* et al. method. Results from the *Lutz* method show a dominant NW trend for shield orientations, which is broadly consistent with the geologic mapping given in Fig. 8b.

method, suggesting some consistency between the regional and local-scale effects of tectonic stress and strain.

4.5. Venus example 2: shield field centered at 31°N, 310°E

The shield field centered at 31°N, 310°E is one of 15 fields analyzed by both Addington (2001) and Ivanov and Head (2004). Based on their geologic mapping efforts, these authors inferred a different stratigraphy with conflicting relative ages of features. Specifically, Addington interpreted the shields as younger than the regional plains, while in contrast, Ivanov and Head interpreted the shields to be older than the regional plains.

In our analysis, we mapped the locations of 70 visible shields in this field as well as surrounding tectonic structures (Fig. 10). Also noted was a distinct geologic contact between two plains units: a low radar albedo unit to the south, and an intermediate radar albedo unit to the north. Results from the Lutz method in the MATLAB tool (Fig. 11a and b) indicate anisotropy with a dominant orientation that peaks between 0 and 20°E. No clear evidence of short-range order is evident in the results from the *Cebriá* et al. method (Fig. 11c and d). The trend revealed with the *Lutz* method is roughly parallel to the E–W trending wrinkle ridges that cross-cut the regional plains units. The orientations of these ridges suggests that the maximum horizontal compressive stress is orthogonal to their strike, a direction that is at odds with the direction of least compressive stress inferred from the shield orientations. We suggest that the shields were formed along pre-existing extensional fractures, and that these fractures were reactivated in compression to form wrinkle ridges following the emplacement of the regional plains. In other words, we infer that the shields predate the regional plains in this instance, a finding more consistent with the Ivanov and Head (2004) interpretation.

5. Discussion

5.1. Assessment of two-point azimuth methods

Initial results from the two methods show promise for the task of evaluating whether anisotropy is present in a volcanic field. Both methods correctly indicate a lack of preferred orientations in the null hypothesis check (Figs. 6 and 7), lending confidence that randomly distributed sets of points will not be over interpreted. In

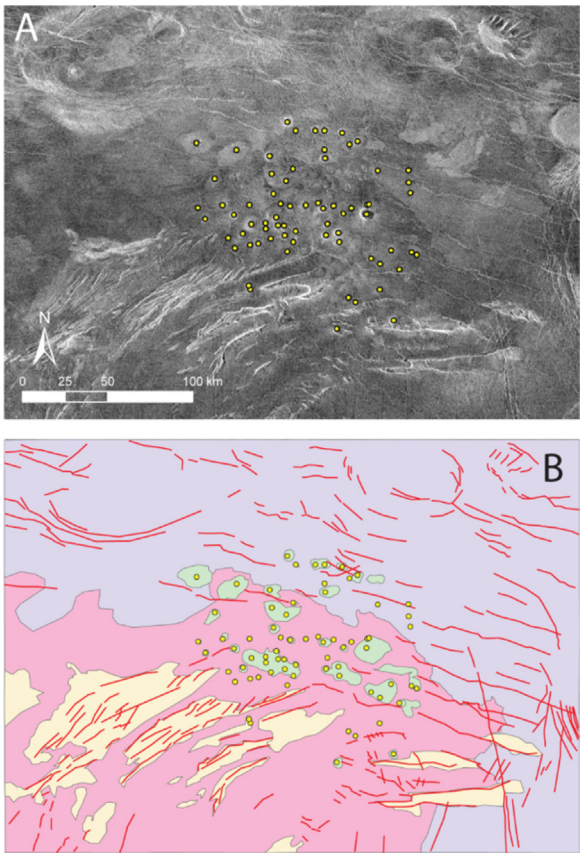

Fig. 10. (a) Magellan left-look SAR image of shield field centered at 31°N, 310°E. The top of the image is north. (b) Simplified geologic map of shield field given above highlighting the distribution of small shields and fractures. Shield locations are given with yellow circles, prominent fractures are marked with solid red lines. (For interpretation of the references to color in this figure legend, the reader is referred to the web version of this article.)

cases where both methods yield the same positive results, one can be reasonably assured that the detected alignments have a basis in reality.

A more challenging case to interpret is one where the alignments detected by the two methods disagree. Two potential causes for such a scenario are (a) situations where volcanic edifices are emplaced into a region with an evolving stress regime, and/or (b) heterogeneities in the spatial distribution of volcanic vents. Assuming that the inferred linkage between aligned edifies and regional stress geometry still holds, edifices emplaced later in the sequence would be responsive to a different stress than the initially emplaced vents, and thus have a different alignment. This challenge highlights the role that time plays in interpreting the stress state. Volcanic classification schemes draw a distinction between monogenetic and polygenetic volcanic fields. Monogenetic fields are composed of vents that experienced a single eruptive episode, whereas polygenetic field consist of volcanoes that have experienced repeated episodes of volcanic activity over a more extended period of time. In a similar manner, a shield field emplaced under uniform conditions we term "unitemporal," meaning all edifices were emplaced under essentially the same stress regime. In contrast, a field that experienced either gradual or abrupt changes in crustal stress geometry would be "multitemporal." It is difficult to put a precise value on the maximum age of a unitemporal field as it is dependent on the rate of change in a particular tectonic setting and magma supply rate. Nevertheless, a significant disagreement between the *Lutz* and *Cebriá* et al. methods is suggestive of a multi-temporal volcanic field.

To help address issues such as heterogeneous distributions, other workers have used clustering analyses to subdivide volcanic fields into various clusters prior to attempting to detect preferred alignments (e.g., Connor, 1990; Connor et al., 1992; Mazzarini and D'Orazio, 2003). Although not uniformly true, some observed clusters differ in age or petrology (e.g., tholeiitic versus alkaline olivine basalt; Connor et al., 1992), with distinct clusters exhibiting notably different regional alignments. We have not applied clustering algorithms to our case studies since they are beyond the scope of this study, but they suggest a potential pathway for future research to better quantify and understand multi-temporal volcanic fields.

5.2. Implications for relative timing

The results indicate that in some cases, the results of the two-point azimuth method can be combined with geologic mapping to provide insight into the relative ages or emplacement order of surface features. In the first venusian shield field near Chernava Colles, anisotropy in the distribution of individual shields is consistent with the orientation of the dominant regional fracture set suggesting that both were responsive to the same stress-strain conditions and that the shields are likely younger than those fractures. In the second shield field centered 31°N, 310°E, shield anisotropy is consistent with the orientation of proximal wrinkle ridges. This suggests that the shields predate those features, and further that the wrinkle ridges may have been formed via re-activation of a pre-existing fracture set.

Given this small group of examples, we are unable to render a decision on the question of whether most shield fields pre-date or post-date nearby regional plains units. But the initial results are encouraging and suggest that the analysis of additional fields may help elucidate this difficult problem.

6. Conclusions

We have developed a MATLAB tool to facilitate application of existing numerical methods in order to improve detection of alignments of vents or edifices in volcanic fields. The program can operate at two different scales: at a whole-field scale using the method of Lutz (1986) and at smaller spatial scales using the method proposed by Cebriá et al. (2011). Initial results on the test cases present here are promising, at least for unitemporal volcanic fields. The method could also be utilized in same manner for other point-like geologic features, such hydrothermal vents, springs, and earthquake epicenters.

Since these programs are made available as standalone executable bundles, an end user need not procure a software license in order to run them. The additional publication of the full source code allows more advanced users to modify the code if needed to suit their particular application. Modification of the code does require a MATLAB software license.

Future work includes exploring cluster detection methods to aid in the identification of sub-populations within a larger grouping. Other proposed techniques for detecting anisotropy, such as strip methods (e.g., Zhang and Lutz, 1989; Amorese et al., 1999; Hammer, 2009), are also candidates for conversion into user-friendly MATLAB models).

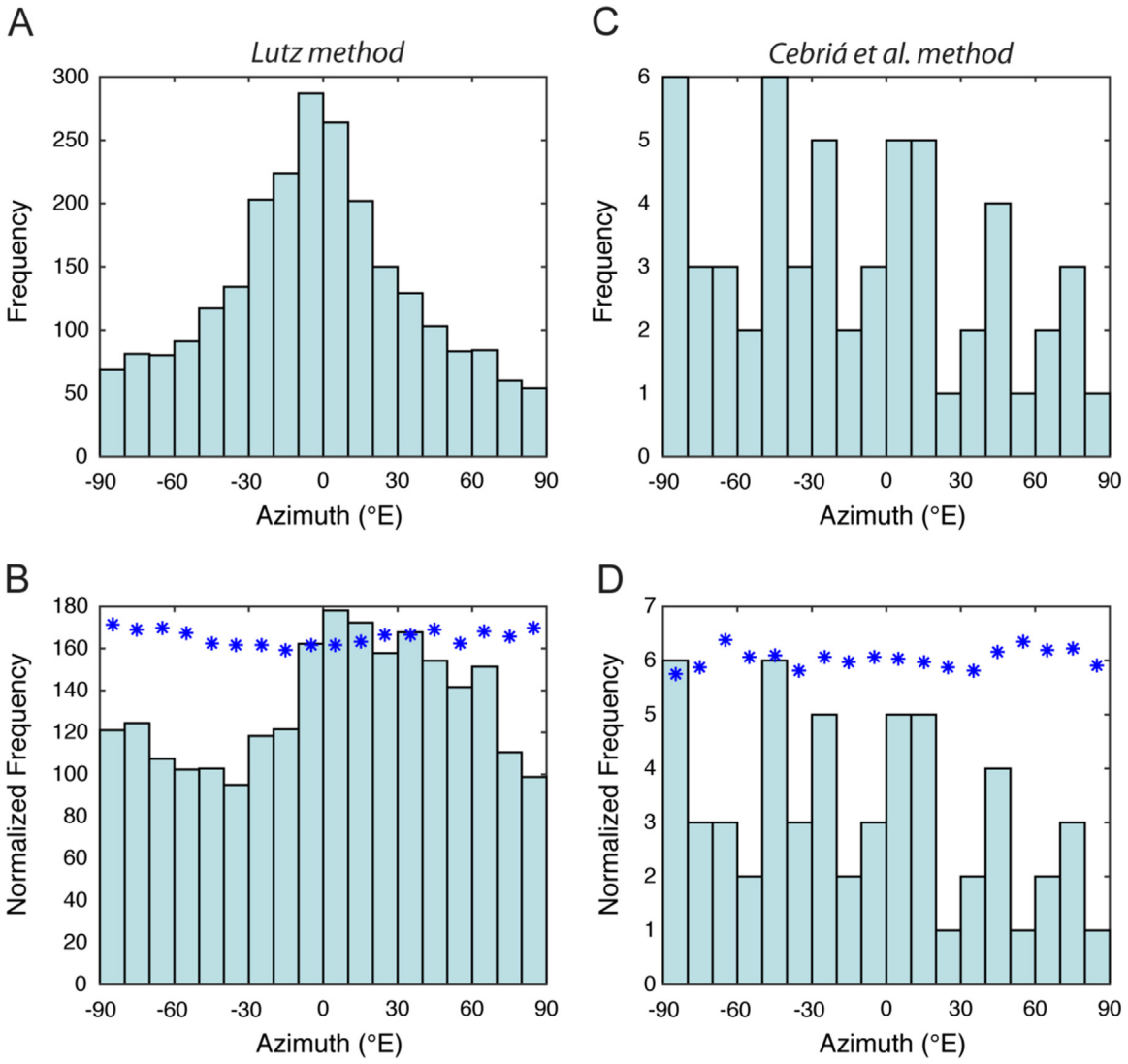

Fig. 11. Results from two-point azimuth methods for shield field centered at 31°N310°E. (a) Histogram of raw azimuth values using two-point azimuth method of Lutz (1986) with 10° bins. (b) Normalized two-point azimuth distribution from a; overlain star symbols in each bin indicate the 95% threshold value. (c) Histogram of raw azimuth values using Cebriá et al. (2011) modified two-point azimuth method. (d) Normalized modified two-point azimuth distribution from c. Overlain star symbols in each bin indicate the 95% threshold value.

Acknowledgments

This work was supported by a Grant from NASA's Planetary Mission Data Analysis Program (P-MDAP, Grant number NNX12AQ72G). The authors thank Jose Cebriá for sharing his randomized set of point data. Constructive reviews from Jacob Richardson and an anonymous reviewer improved both the manuscript and the code. This work benefited from advice given through the BU MSSP (Master of Science in Statistical Practice) statistical consulting service by students Jun Li, Jingshu Wu, Lina Zhou, and Frank Giron under the supervision of Prof. Eric Kolaczyk.

Appendix A. Supplementary material

Supplementary data associated with this article can be found in the online version at http://dx.doi.org/10.1016/j.cageo.2016.04.012, including source code and pre-compiled binaries for Windows 7 and Mac OS X 10.10.5.

References

Addington, E.A., 2001. A stratigraphic study of small volcano clusters on Venus. Icarus 149, 16–36.
Amorese, D., Lagarde, J.-L., Laville, E., 1999. A point pattern analysis of the distribution of earthquakes in Normandy (France). Bull. Seismol. Soc. Am. 89, 742–749.
Anderson, E.M., 1951. The Dynamics of Faulting and Dyke Formation With Applications to Britain. Oliver and Boyd, Edinburgh.
Aubele, J.C., Sliuta, E.N., 1990. Small domes on Venus: characteristics and origin. Earth Moon Planets 50, 493–532.
Basaltic Volcanism Study Project, 1981. Basaltic volcanism on the terrestrial planets. Pergamon Press, Inc., New York.
Bender, K.C., Senske, D.A., Greeley, R., 2000. Geologic map of the Carson Quadrangle (V-43), Venus, U.S. Geological Survey Geologic Investigations Series Map I-2620.
Bleacher, J.E., Glaze, L.S., Greeley, R., Hauber, E., Baloga, S.M., Sakimoto, S.E.H., Williams, D.A., Glotch, T.D., 2009. Spatial and alignment analyses for a field of small volcanic vents south of Pavonis Mons and implications for the Tharsis province, Mars. J. Volcanol. Geotherm. Res. 185, 96–102.
Cebriá, J.M., Martín-Escorza, C., López-Ruiz, J., Morán-Zenteno, D.J., Martiny, B.M., 2011. Numerical recognition of alignments in monogenetic volcanic areas: examples from the Michoacán-Guanajuato Volcanic Field in Mexico and Calatrava in Spain. J. Volcanol. Geotherm. Res. 201, 73–82.
Connor, C.B., 1990. Cinder cone clustering in the TransMexican Volcanic Belt: implications for structural and petrologic models. J. Geophys. Res. 95, 19,395–319,405.

Connor, C.B., Condit, C.D., Crumpler, L.S., Aubele, J.C., 1992. Evidence of regional structural controls on vent distribution: Springerville Volcanic Field, Arizona. J. Geophys. Res. 97, 12,349–312,359.
Connor, C.B., Conway, F.M., 2000. Basaltic volcanic fields. In: Encyclopedia of Volcanoes, pp. 331–343.
Crumpler, L., Aubele, J.C., 2000. Volcanism on Venus, Encyclopedia of Volcanoes. Academic Press, San Diego, pp. 727–770.
Crumpler, L.S., Aubele, J.C., Senske, D.A., Keddie, S.T., Magee, K.P., Head, J.W., 1997. Volcanoes and centers of volcanism on Venus. In: Bougher, S.W., Hunten, D.M., Phillips, R.J. (Eds.), Venus II.. University of Arizona Press, Tucson, pp. 697–756.
Ernst, R.E., Head, J.W., Parfitt, E., Grosfils, E., Wilson, L., 1995. Giant radiating dyke swarms on Earth and Venus. Earth-Sci. Rev. 39, 1–58.
Guest, J.E., Bulmer, M.H., Aubele, J., Beratan, K., Greeley, R., Head, J.W., Michaels, G., Weitz, C., Wiles, C., 1992. Small volcanic edifices and volcanism in the plains of Venus. J. Geophys. Res. 97, 15949.
Hammer, O., 2000. Spatial organization of tubercles and terrace lines in *Paradoxides forchhammeri* - evidence of lateral inhibition. Acta Palaeontol. Pol. 45, 251–270.
Hammer, O., 2009. New statistical methods for detecting point alignments. Comput. Geosci. 35, 659–666.
Hodges, C.A., Moore, H.J., 1994. Atlas of Volcanic Landforms on Mars, U.S. Geological Survey Professional Paper. U.S. Gov. Printing Office, Washington, D.C., p. 194.
Ivanov, M.A., Head, J.W., 2004. Stratigraphy of small shield volcanoes on Venus: criteria for determining stratigraphic relationships and assessment of relative age and temporal abundance. J. Geophys. Res., 109.
Kear, D., 1964. Volcanic alignments north and west of New Zealand's central volcanic region. N. Z. J. Geol. Geophys. 7, 24–44.
Lee, D.-T., Schachter, B.J., 1980. Two algorithms for constructing a Delaunay triangulation. Int. J. Comput. Inf. Sci. 9, 219–242.
Lutz, T.M., 1986. An analysis of the orientations of large scale crustal structures: a statistical approach based on areal distributions of pointlike features. J. Geophys. Res. 91, 421–434.
Lutz, T.M., Gutmann, J.T., 1995. An improved method for determining and characterizing alignments of pointlike features and its implications for the Pinacate volcanic field, Sonora, Mexico. J. Geophys. Res. 100, 17,659–617,670.
Mazzarini, F., D'Orazio, M., 2003. Spatial distribution of cones and satellite-detected lineaments in the Pali Aike Volcanic Field (southernmost Patagonia): insights into the tectonic setting of a Neogene rift system. J. Volcanol. Geotherm. Res. 125, 291–305.
Nakamura, T., 1977. Volcanoes as possible indicators of tectonic stress orientation - Principals and proposal. J. Volcanol. Geotherm. Res. 2, 1–16.
Odé, H., 1957. Mechanical analysis of the dike pattern of the Spanish Peaks area, Colorado. Geol. Soc. Am. Bull. 68, 567–576.
Phillips, R.J., Raubertas, R.F., Arvidson, R.A., Sarkar, I.C., Herrick, R.R., Izenburg, N., Grimm, R.E., 1992. Impact craters and Venus resurfacing history. J. Geophys. Res. 97, 15,923–915,948.
Richardson, J.A., Bleacher, J.E., Glaze, L.S., 2013. The volcanic history of Syria Planum, Mars. J. Volcanol. Geotherm. Res. 252, 1–13.
Schaber, G.G., Strom, R.G., Moore, H.J., Soderblom, L.A., Kirk, R.L., Chadwick, D.J., Dawson, D.D., Gaddis, L.R., Boyce, J.M., Russel, J., 1992. Geology and distribution of impact craters on Venus: what are they telling us? J. Geophys. Res. 97, 13257–13301.
Strom, R.G., Schaber, G.G., Dawsow, D.D., 1994. The global resurfacing of Venus. J. Geophys. Res. 99, 10,899–810,926.
Thompson, A.M., Hager, G.M., 1977. Lineament studies in structural interpretation of a stabilized orogenic region: Appalachian Piedmont, Delaware and adjacent Pennsylvania, In: Podwysocki, M.H., Earle, J.L. (Eds.), Proceedings of the Second International Conference on New Basement Tectonics, Newark, DE, pp. 74–85.
Weisstein, E.W., 2016. Triangle Point Picking, from MathWorld – A Wolfram Web Resource, ⟨http://mathworld.wolfram.com/TrianglePointPicking.html⟩.
Zhang, D., Lutz, T., 1989. Structural control of igneous complexes and kimerlites: a new statistical method. Tectonophysics 159, 137–148.